Coupling of Hydrogen Bonding to Chromophore Conformation and Function in Photoactive Yellow Protein †

ARTICLE *in* BIOCHEMISTRY · DECEMBER 2000

Impact Factor: 3.02 · DOI: 10.1021/bi0009946 · Source: PubMed

Coupling of Hydrogen Bonding to Chromophore Conformation and Function in Photoactive Yellow Protein†

Ronald Brudler,*,‡ Terrence E. Meyer,§ Ulrich K. Genick,‡ Savitha Devanathan,§ Tammy T. Woo,‡ David P. Millar,‡ Klaus Gerwert,|| Michael A. Cusanovich,§ Gordon Tollin,§ and Elizabeth D. Getzoff*,‡

Department of Molecular Biology and Skaggs Institute for Chemical Biology, The Scripps Research Institute, La Jolla, California 92037, Department of Biochemistry, University of Arizona, Tucson, Arizona 85721, and Lehrstuhl für Biophysik, Ruhr-Universität Bochum, D-44780 Bochum, Germany

Received May 1, 2000; Revised Manuscript Received July 24, 2000

ABSTRACT: To understand in atomic detail how a chromophore and a protein interact to sense light and send a biological signal, we are characterizing photoactive yellow protein (PYP), a water-soluble, 14 kDa blue-light receptor which undergoes a photocycle upon illumination. The active site residues glutamic acid 46, arginine 52, tyrosine 42, and threonine 50 form a hydrogen bond network with the anionic *p*-hydroxycinnamoyl cysteine 69 chromophore in the PYP ground state, suggesting an essential role for these residues for the maintenance of the chromophore's negative charge, the photocycle kinetics, the signaling mechanism, and the protein stability. Here, we describe the role of T50 and Y42 by use of site-specific mutants. T50 and Y42 are involved in fine-tuning the chromophore's absorption maximum. The high-resolution X-ray structures show that the hydrogen-bonding interactions between the protein and the chromophore are weakened in the mutants, leading to increased electron density on the chromophore's aromatic ring and consequently to a red shift of its absorption maximum from 446 nm to 457 and 458 nm in the mutants T50V and Y42F, respectively. Both mutants have slightly perturbed photocycle kinetics and, similar to the R52A mutant, are bleached more rapidly and recover more slowly than the wild type. The effect of pH on the kinetics is similar to wild-type PYP, suggesting that T50 and Y42 are not directly involved in any protonation or deprotonation events that control the speed of the light cycle. The unfolding energies, 26.8 and 25.1 kJ/mol for T50V and Y42F, respectively, are decreased when compared to that of the wild type (29.7 kJ/mol). In the mutant Y42F, the reduced protein stability gives rise to a second PYP population with an altered chromophore conformation as shown by UV/visible and FT Raman spectroscopy. The second chromophore conformation gives rise to a shoulder at 391 nm in the UV/visible absorption spectrum and indicates that the hydrogen bond between Y42 and the chromophore is crucial for the stabilization of the native chromophore and protein conformation. The two conformations in the Y42F mutant can be interconverted by chaotropic and kosmotropic agents, respectively, according to the Hofmeister series. The FT Raman spectra and the acid titration curves suggest that the 391 nm form of the chromophore is not fully protonated. The fluorescence quantum yield of the mutant Y42F is 1.8% and is increased by an order of magnitude when compared to the wild type.

Light is an important source of information for a variety of organisms in order to respond to environmental changes. Photoactive yellow protein (PYP),[1] first isolated from the phototrophic bacterium *Ectothiorhodospira halophila* (*1*) and later also found in other purple bacteria (*2*−*4*), is a 14 kDa water-soluble, cytoplasmic blue-light receptor, presumably mediating negative phototaxis in some species to avoid UV radiation damage (*5*). In *Rhodospirillum centenum*, the PYP−phytochrome hybrid is involved in regulation of chalcone synthase (*4*). PYP's chromophore is a *p*-hydroxycinnamoyl anion covalently bound to C69 via a thioester linkage (*6*, *7*). PYP undergoes a photocycle upon illumination, involving *trans*−*cis* isomerization of the chromophore, similar to the photocycles from the well-known membrane proteins bacteriorhodopsin, halorhodopsin, and the two sensory rhodopsins from the unrelated archaebacterium *Halobacterium salinarum* (*8*, *9*). In the light cycle, the ground-state P (λ_{max} = 446 nm) is converted into the recently identified intermediates I_0 (≤2 ps) and then $I^{\ddagger}_0$ (220 ps), both absorbing at ∼510 nm (*10*, *11*). $I^{\ddagger}_0$ proceeds in about 3 ns into the intermediate I_1 (λ_{max} = 465 nm), which is followed by the blue-shifted intermediate I_2 (λ_{max} = 350 nm) in about 200 μs. I_2 returns to the ground state in about 140 ms. The

† This work was supported by grants from the NIH to E.D.G. (GM37684) and the NSF to the Tucson laboratory (MCB-9722781), a scholarship from the Boehringer Ingelheim Fonds to U.K.G., and a fellowship from the Deutsche Forschungsgemeinschaft to R.B.

* To whom correspondence should be addressed. E-mail: edg@scripps.edu or rbrudler@scripps.edu.

‡ The Scripps Research Institute.

§ University of Arizona.

|| Ruhr-Universität Bochum.

[1] Abbreviations: EDTA, ethylenediaminetetraacetic acid; FPLC, fast-performance liquid chromatography; FT, Fourier transform; HEPES, *N*-(2-hydroxyethyl)piperazine-*N*′-2-ethanesulfonic acid; IPTG, isopropyl β-D-thiogalactopyranoside; MES, 2-(*N*-morpholino)ethanesulfonic acid; PCR, polymerase chain reaction; PYP, photoactive yellow protein; SDS−PAGE, sodium dodecyl sulfate−polyacrylamide gel electrophoresis.

10.1021/bi0009946 CCC: $19.00
Published on Web 10/12/2000

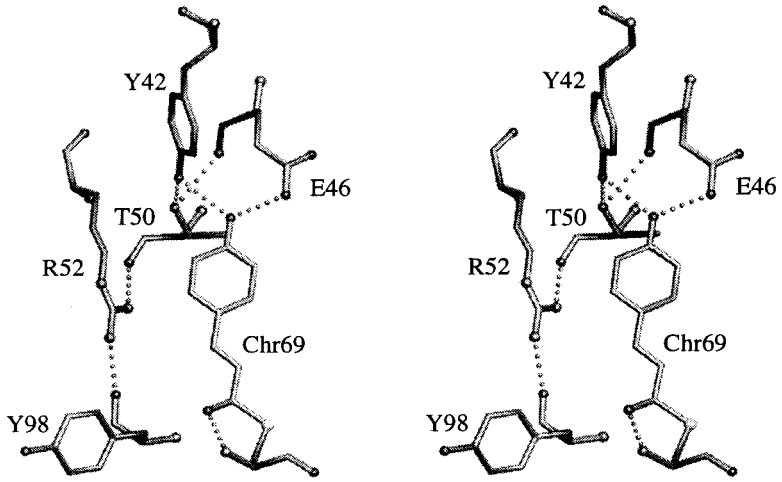

FIGURE 1: Stereoview of the three-dimensional arrangement of active site residues in the PYP ground state (*12*). Hydrogen bonds are indicated by dotted lines.

availability of high-resolution structural information for the PYP ground state (*12, 13*), the intermediate I_2 (*14*), and a preceding early intermediate (*15, 16*) as well as the feasibility of site-directed mutagenesis (*17*−*20*) and reconstitution of chromophore variants (*21, 22*) makes PYP an ideal system to study the conversion of light energy into a biological signal in atomic detail.

The 1.4 Å X-ray structure of PYP in the dark or ground state (*12*) shows that the chromophore is buried in a hydrophobic core and tethered to the protein by a network of hydrogen bonds (Figure 1). The phenolate oxygen of the chromophore hydrogen bonds with the hydroxyl group of Y42 and the protonated carboxylate of E46. The side-chain oxygen of T50 hydrogen bonds both with the main-chain carbonyl oxygen of E46 and with the OH group of Y42. In addition, the main-chain oxygen of T50 forms a hydrogen bond with the side chain of R52, which shields the chromophore from solvent and undergoes major rearrangement during the photocycle (*14*). The location of these amino acids suggests that they are essential for the maintenance of the chromophore's negative charge, the photocycle kinetics, the signaling mechanism, and the protein stability. The influence of residues E46 and R52 on the spectral properties and the photocycle kinetics of PYP was examined previously (*17, 20*). Here, we characterize the role of the amino acids T50 and Y42 by aid of T50V and Y42F mutants.

MATERIALS AND METHODS

Site-Directed Mutagenesis. Mutagenesis was performed by a PCR-based approach as implemented in the QuickChange kit (Stratagene) and with the PYP gene in a pET-20b vector (Novagen) as the template (*17*). The sequences for the mutagenic primers were 5′GAGGGCGACATC*GT*CGGCCGCGACCC3′ for the T50V mutation and 5′GCAACATCCTTCAGT*T*CAACGCCGCGGAG3′ for Y42F. The mutations were confirmed at the DNA level by automated sequencing with an Applied Biosystems sequencer.

Protein Production and Purification. Escherichia coli cells of strain BL21 (DE3) (Novagen) were transformed with the pET-20b vector including the mutated PYP gene and grown in a M9ZB medium (*23*) at 37 °C until they reached an absorbance of ∼0.5 at 650 nm. Expression of apo-PYP was induced by addition of IPTG to the medium to a final concentration of 0.1 mM. After 3 h, the cells were separated from the apo-PYP-containing medium by centrifugation. Chemical attachment of the activated chromophore in the growth medium, concentration of the medium by lateral flow filtration, and purification of the PYP holoprotein by $(NH_4)_2SO_4$ precipitation were performed as described previously (*17*), except that the $(NH_4)_2SO_4$ concentration was reduced to 55% to prevent excessive precipitation of the mutant PYP proteins. Further purification included three FPLC steps. The 55% ammonium sulfate precipitate was removed by centrifugation, and the sample was applied to a butyl-Sepharose hydrophobic interaction column (Pharmacia). The column was eluted with Tris−EDTA buffer (50 mM Tris-HCl, 2 mM EDTA, pH 7.5) containing a concentration gradient of 1.25−0 M $(NH_4)_2SO_4$. Fractions with an absorbance ratio A_{280}/A_{458} <10 were pooled, dialyzed overnight against 20 mM Tris-HCl and 2 mM EDTA, pH 7.5, concentrated to 10 mL by membrane filtration with a YM10 membrane (Amicon), and loaded onto a Poros-HQ anion-exchange column (PerSeptive Biosystems). The column was eluted with a concentration gradient of 0−1.0 M NaCl in Tris−EDTA buffer. The yellow fractions were pooled, concentrated to 2−4 mL by membrane filtration, and finally applied to a Superdex 75 gel filtration column (Pharmacia). PYP was eluted with Tris−EDTA buffer containing 150 mM NaCl. Purity was checked by SDS−PAGE. Fractions with an absorbance ratio A_{280}/A_{458} ∼0.5 were pooled and dialyzed overnight against 20 mM HEPES buffer, pH 7.0.

UV/Vis Spectroscopy. Static UV/vis spectra were recorded on a diode array spectrophotometer (Hewlett-Packard, model 8453). The laser flash photolysis setup for time-resolved UV/vis spectroscopy and data analysis procedures have been described elsewhere (*8, 24*). Kinetic measurements at different pH values were performed according to ref *17*.

Fluorescence Spectroscopy. Fluorescence excitation and emission spectra were recorded on an SLM 8100 spectrofluorometer (Spectronics Instruments). Measurements of the fluorescence quantum yield Φ were made relative to fluorescein according to ref *25*. A value of 0.92 was used for the fluorescein quantum yield (*26*). The error for Φ was estimated to be ±8%, using standard methods for error propagation.

FT Raman Spectroscopy. FT Raman spectroscopy was performed with an FRA 106 FT Raman module connected to an IFS 88 spectrometer (Bruker). The home-built sample holder consisted of a mirrored Suprasil quartz sphere (10 mm diameter) with a central hole. The geometry and the reflecting surface of the sphere optimize the intensity of the Raman scattering. The sample (4 μL of 40 mg/mL PYP in 20 mM HEPES buffer, pH 7.0) was pipetted into a quartz capillary (2 mm outer diameter) and put into the sphere. The sphere sat in an adjustable temperature aluminum block on an xyz translatable table that allows the superposition of the foci of the exciting laser beam and the collecting lens on the sample. The sample was excited with a Nd:YAG laser (Adlas) at 1064 nm (laser spot at the sample 100 μm). A total of 20−60 spectra, each consisting of 200 scans, were averaged to improve the signal-to-noise ratio. The spectral resolution was 2 ± 1 cm^{-1}. All measurements were performed at room temperature (22 °C). The spectra were corrected by subtraction of a buffer spectrum (20 mM HEPES, pH 7.0) measured under identical conditions.

Protein Stability and Circular Dichroism. Protein stability was assessed by denaturation of 1 μM solutions of PYP in 20 mM Tris-HCl buffer, pH 7.5, plus 40 mM NaCl, with increasing concentrations of guanidine hydrochloride (USB, ultrapure) following the method of Pace (*8*, *27*). Unfolding was monitored by loss of absorbance at 450 nm with a diode array spectrophotometer (Hewlett-Packard, model 8452) and by changes in the molar ellipticity at 222 nm (AVIV Instruments modified Cary 60 spectropolarimeter).

X-ray Crystallography. PYP T50V and Y42F were crystallized in ~2.5 M $(NH_4)_2SO_4$ and 20 mM Hepes, pH 7.0, from microseeds of wild-type protein as described in ref *12*. Like wild-type PYP, crystals grew as long hexagonal rods (50−300 × 500−1000 μm) in space group $P6_3$. Unit cell dimensions were $a = b = 67.8$ Å and $c = 39.4$ Å for T50V and $a = b = 66.0$ Å and $c = 40.5$ Å for Y42F. High-resolution data were collected in each case on a single crystal by using separate low- and high-resolution runs. The data were processed with Denzo and Scalepack (*28*). Because of the unit cell change in T50V, molecular replacement was performed with the AMoRe suite (*29*). The high-resolution structures were refined with SHELX97 (*30*), starting from the 1.4 Å resolution structure of wild-type PYP (*12*) (PDB code 2PHY), which is the model used here for comparison with the PYP T50V and Y42F structures. Diffraction data for T50V were collected at the Cornell High Energy Synchrotron Source (CHESS) at beamline F1, using an X-ray wavelength of 0.9188 Å and a 2 × 2 Quantum 4 ADSC X-ray detector. Diffraction data for Y42F were collected at the Stanford Synchrotron Radiation Laboratory (SSRL) at beamline 7-1, which is operated at an X-ray wavelength of 1.08 Å and equipped with Mar Research image plates.

RESULTS

Steady-State UV/Vis Spectroscopy of the PYP Mutants T50V and Y42F. Effects of Denaturing, Chaotropic and Kosmotropic Agents, and pH. The absorption maxima of the PYP mutants T50V and Y42F are located at 457 and 458 nm, respectively (Figure 2). They are red shifted by 540 and 587 cm^{-1}, respectively, relative to the wild type (446 nm) in agreement with ref *18*. A remarkable feature of Y42F is a shoulder at 391 nm. Unlike the mutant M100A (*19*), the spectrum of Y42F was unaltered by overnight incubation in the dark and exposure to room light. To further characterize the spectral shoulder of Y42F, we studied the effects of denaturing, chaotropic and kosmotropic agents, and pH.

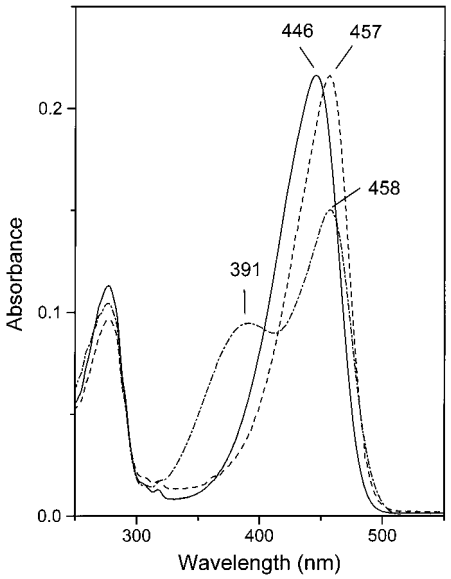

FIGURE 2: UV/vis absorption spectra of wild-type PYP (solid line), T50V (dashed line), and Y42F (dash-dotted line) at room temperature in 20 mM HEPES buffer, pH 7.0.

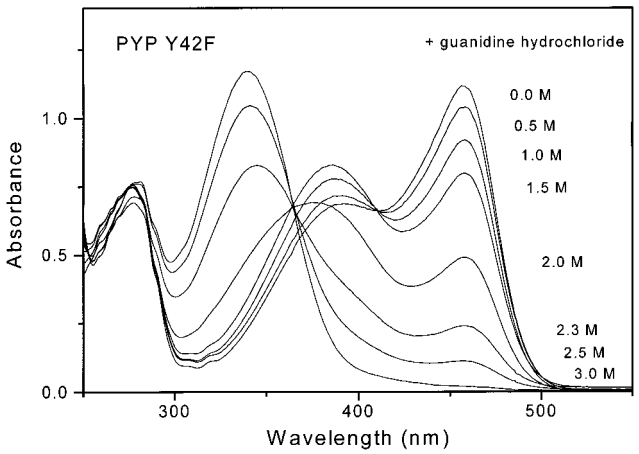

FIGURE 3: Guanidine hydrochloride denaturation of Y42F in 20 mM HEPES buffer, pH 7.0, as monitored by UV/vis absorption spectra.

The effect of the denaturant guanidine hydrochloride on the Y42F mutant is shown in Figure 3. The 458 nm peak is partially converted to the 391 nm peak at a midpoint of about 1.1 M guanidine hydrochloride and then to the denatured 340 nm species at a midpoint of about 2.2 M guanidine hydrochloride. In contrast, the 446 nm form of the wild-type protein is directly converted into the denatured 340 nm species at about 2.7 M guanidine hydrochloride (not shown). The unfolding energies, ΔG_{unfold}, of Y42F and T50V were determined by monitoring changes in the UV and visible circular dichroism as a function of the concentration of guanidine hydrochloride according to ref *27* and yielded values of 25.1 and 26.8 kJ/mol, respectively. ΔG_{unfold} for wild-type PYP is 29.7 kJ/mol (*17*).

Figure 4 shows the influence of pH on the absorption maximum for T50V and Y42F. The lower stability of these

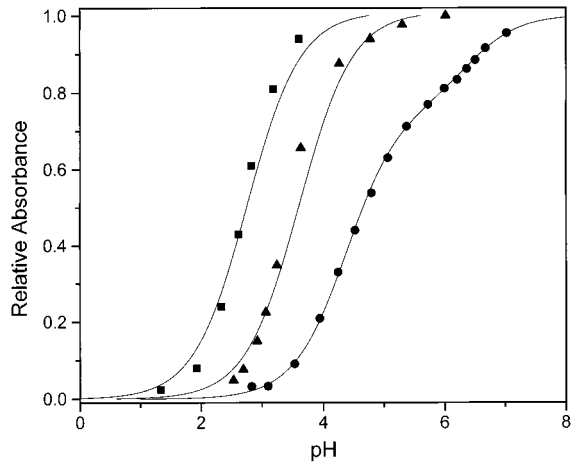

FIGURE 4: Acid titration curves of wild-type PYP (squares), T50V (triangles), and Y42F (circles), as monitored by UV/vis absorbance at the wavelength maxima. The solid lines represent the fitted curves. Wild-type PYP has a pK_a of 2.7, and T50V has a pK_a of 3.6. Y42F shows a biphasic transition with pK_as of 4.4 (amplitude 75%) and 6.4 (amplitude 25%).

mutants in guanidine hydrochloride is also reflected in the higher apparent pK_a values of the chromophore when compared to the wild type (pK_a 2.7) (*1*). In T50V the chromophore has an apparent pK_a of 3.6, and in Y42F it shows clearly a biphasic transition with pK_as of 4.4 and 6.4.

To further test the stability of the Y42F mutant, we also studied the effects of chaotropic and kosmotropic (=anti-chaotropic) agents. The kosmotrope $(NH_4)_2SO_4$ stabilizes the main peak at 458 nm by reducing the 391 nm form, whereas the chaotrope NH_4Cl destabilizes the 458 nm peak and increases the sideband at 391 nm (Figure 5). The same effects were observed for a number of other chaotropes and kosmotropes. The strength of the chaotropic ($SCN^- > ClO_4^- > I^- > Br^- > Cl^-$) and kosmotropic effects ($SO_4^{2-} > HPO_4^{2-} > F^-$; F^- had almost no effect, even at 4 M concentrations) corresponded with the Hofmeister series (*31*, *32*). We also tested different cations [Na_2SO_4, $(NH_4)_2SO_4$, NaCl, NH_4Cl]. The ammonium salts had a stronger kosmotropic or chaotropic effect, respectively, than the corresponding sodium salts.

FT Raman Spectroscopy. Raman spectroscopy is a sensitive tool to selectively monitor the structural changes of chromophores in proteins (see, for example, ref *33*) and was applied to further characterize the PYP mutants T50V and Y42F (Figure 6). The FT Raman spectrum of wild-type PYP in the ground state (Figure 6a) exhibits bands at 1555, 1530, 1493, 1439, 1282, 1163, 1057, 1043, 1003, and 983 cm^{-1}, in very good agreement with a previous resonance Raman study (*34*). This demonstrates that even preresonant excitation at 1064 nm allows observation of Raman scattering of the PYP chromophore. Differences between the FT and the resonance Raman spectrum are mainly related to band intensities. In addition, the broad resonance Raman band at 1288 cm^{-1} with a shoulder at ~1300 cm^{-1} (*34*) appears split in the FT Raman spectrum with peaks at 1282 and 1306 cm^{-1}. A small band at 1633 cm^{-1} (*34*) does not exceed the noise level in the FT Raman spectrum. Instead, a stronger band is seen at 1667 cm^{-1}. The FT Raman spectra of PYP wild type and the mutant T50V are very similar, with only minor band shifts of at most 4 cm^{-1} (Figure 6a,b). In contrast,

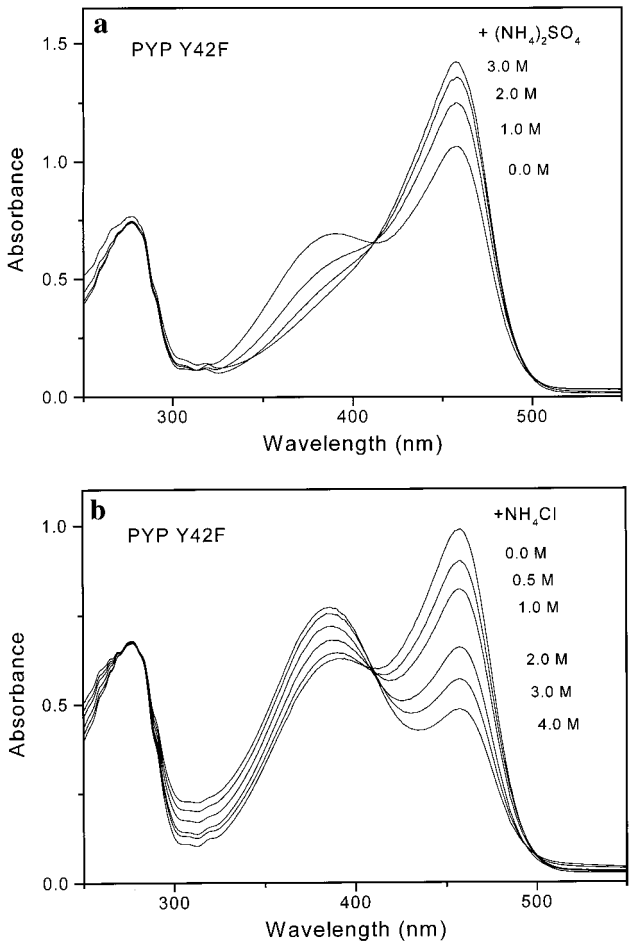

FIGURE 5: (a) Effect of increasing concentrations of the kosmotrope $(NH_4)_2SO_4$ on the absorption spectrum of Y42F in 20 mM HEPES buffer, pH 7.0 at room temperature. (b) Effect of increasing concentrations of the chaotrope NH_4Cl on the absorption spectrum of Y42F in 20 mM HEPES buffer, pH 7.0 at room temperature.

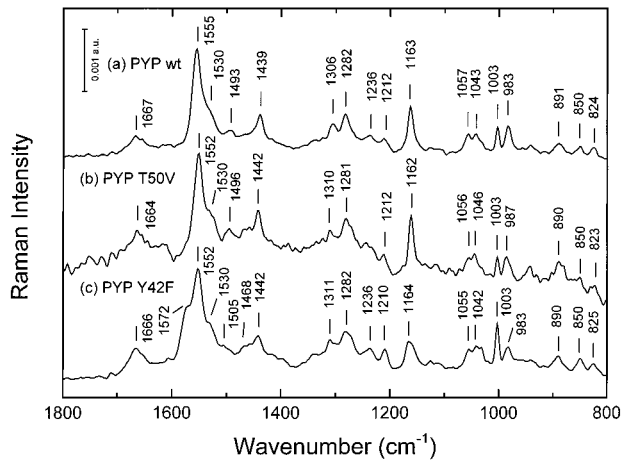

FIGURE 6: FT Raman spectra of (a) wild-type PYP, (b) T50V, and (c) Y42F in 20 mM HEPES, pH 7.0 at room temperature.

the Raman spectrum of Y42F is very different from the wild-type spectrum (Figure 6a,c). The main peak at 1555 cm^{-1} (1552 cm^{-1} in Y42F) has a large shoulder at 1572 cm^{-1}, which is missing for the wild type.

The effects of the kosmotrope $(NH_4)_2SO_4$ and the chaotrope NH_4Cl on the main Raman bands of Y42F at 1552 and 1572 cm^{-1} are analogous to the effects of these agents

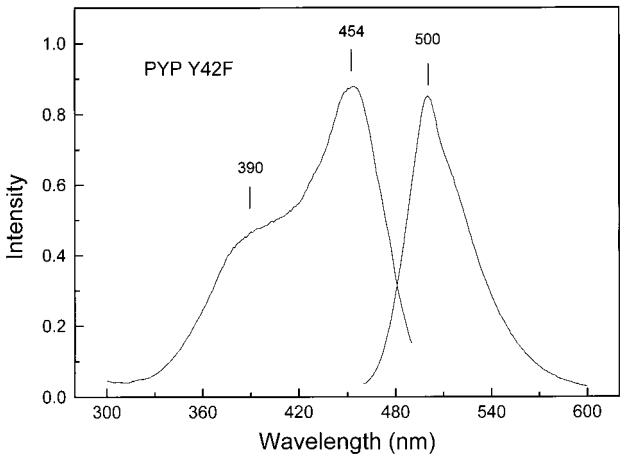

FIGURE 7: Fluorescence excitation and emission spectra of the PYP mutant Y42F in 20 mM HEPES buffer, pH 7.0.

on the UV/vis spectra. $(NH_4)_2SO_4$ stabilizes the main peak at 1552 cm^{-1} and decreases the shoulder at 1572 cm^{-1}. In contrast, NH_4Cl increases the 1572 cm^{-1} peak intensity and reduces the maximum at 1552 cm^{-1}.

Fluorescence Spectroscopy. The fluorescence excitation spectrum (fluorescence emission monitored at 500 nm) and the emission spectrum (fluorescence excitation at 446 nm) of the mutant Y42F are shown in Figure 7. The emission maximum of wild-type PYP at 495 nm (*25*) is slightly shifted to 500 nm in the mutant. The emission spectrum in Figure 7 is very similar to wild-type PYP (*25*). Comparison with the UV/vis absorption spectrum (Figure 2) shows that there is a strong correlation between the location of the absorption maxima and the fluorescence excitation maxima. Remarkably, the 391 nm spectral shoulder (Figure 2) has a counterpart in the excitation spectrum at about 390 nm (Figure 7). The emission spectrum of Y42F does not change in response to the excitation wavelength between 320 and 450 nm, except in intensity (not shown). The fluorescence shows a linear intensity decrease in response to diluting the sample from 0.1 mM to 1 μM (not shown). The fluorescence quantum yields Φ were determined to be 1.8% and 0.42% for Y42F and T50V, respectively. Φ of wild-type PYP is about 0.2% (*21*, *25*).

Laser Flash Photolysis. The substitution of T50 by valine increases the rate of photobleaching and decreases the rate of subsequent recovery of color (Figure 8). The rate constant for the $I_1 \rightarrow I_2$ transition increases approximately 3-fold to ~10 ms^{-1} at pH 7.0 (3.1−3.9 ms^{-1} for wild type) (*17*); the $I_2 \rightarrow P$ conversion is slowed by a factor of approximately 5 to ~1 s^{-1} (4.9−6.7 s^{-1} in wild type) (*17*). As for wild-type PYP (*17*), the rate constants for both transitions are only slightly affected by pH in the pH range from 5 to 10 (Figure 8). The rate constant for the $I_1 \rightarrow I_2$ conversion decreases about 3-fold in this pH range. The $I_2 \rightarrow P$ transition shows a bell-shaped pH dependence like PYP wild type with two apparent pK_as at 6.1 and 9.9 (6.4 and 9.4 in wild type) (*17*) and a 3-fold change in rate constant between pH 5 and pH 10. The maximal rate constant for this reaction occurs at pH 7.9 as in wild type. The quantum yield is essentially unaffected by the T50V mutation, as judged by the magnitude of the laser-induced photomultiplier signal. This is in agreement with the only slightly changed fluorescence quantum yield (see above).

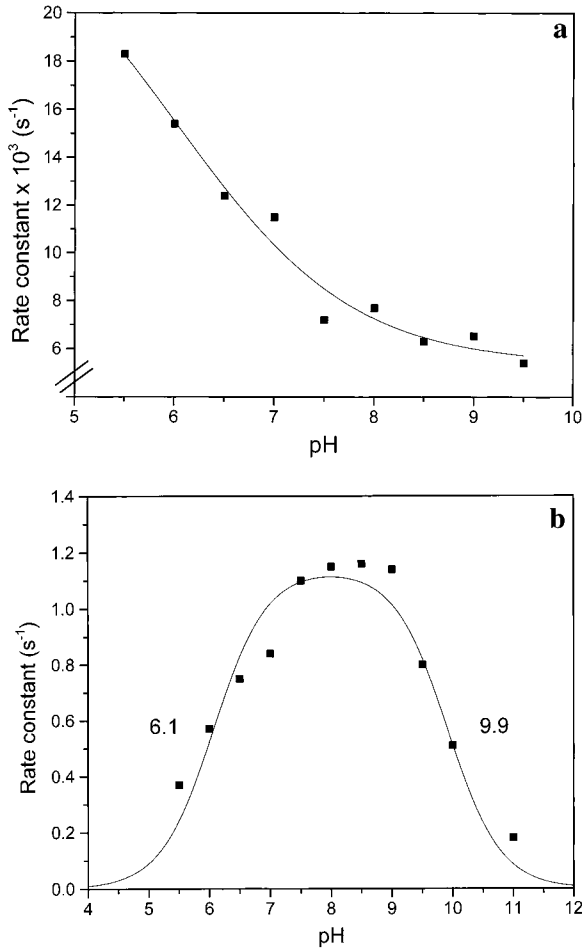

FIGURE 8: Effect of pH on the kinetics of the (a) $I_1 \rightarrow I_2$ and the (b) $I_2 \rightarrow P$ transition of T50V. The buffers were 20 mM MES (pH 5.0−6.5), 20 mM HEPES (pH 6.5−8.5), and glycine (pH 8.5−10.0). The data in (b) were fitted using the equation $k_{obs} = k_{max}/(1 + 10^{pK_1-pH})(1 + 10^{pH-pK_2})$ with the fitted parameters $k_{max} = 1.14$, p$K_1 = 6.1$, and p$K_2 = 9.9$. The data in (a) were not fitted due to the lack of an obvious starting and end point of the curve.

Upon excitation at 445 nm, the $I_1 \rightarrow I_2$ transition in the Y42F mutant is accelerated when compared to the wild type and was too fast to measure with our apparatus (microsecond time resolution) at room temperature and pH 7.0. However, the rate constant at pH 9 was found to be 3.4 ms^{-1} and at pH 10 was 1 ms^{-1}. The $I_2 \rightarrow P$ transition has a rate constant of ~1.4 s^{-1} at pH 7.0 and is slowed about 4-fold in comparison to the wild-type protein (Figure 9). The effects of pH on the rate constant for the recovery reaction are similar to those of T50V and the wild type (*17*). The curve is bell-shaped (Figure 9) with two apparent pK_as at 6.9 and 9.7 (6.4 and 9.4 in wild type). The rate constant varies ~12-fold over the pH range 5−10 and is maximal at pH 8.2 as compared to pH 7.9 in wild-type PYP. Photocycling initiated by light excitation at 450 nm or at 365 nm reflected the relative absorbance at the two wavelengths and shared similar kinetics, suggesting that both chromophore conformations are in *trans*.

X-ray Crystallography. Crystallization of the T50V and Y42F mutants was performed at ~2.5 M ammonium sulfate concentrations according to ref *12*. Under these conditions, the main absorption peak at 458 nm in the Y42F mutant is stabilized, and the 391 nm shoulder is almost completely

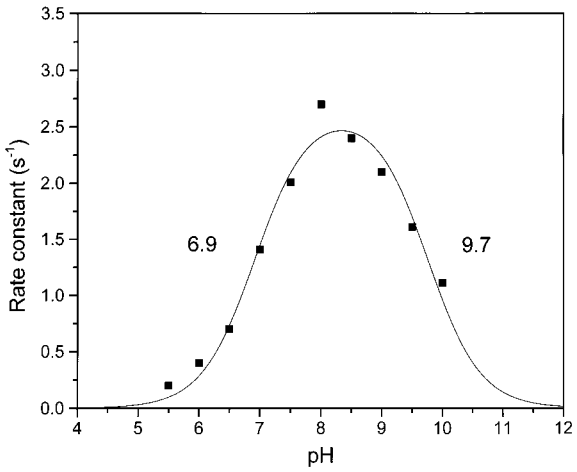

FIGURE 9: Effect of pH on the kinetics of the $I_2 \rightarrow P$ transition of Y42F. Buffers were the same as in Figure 8. The data were fitted with the equation from Figure 8, using the fitted parameters $k_{max} = 2.66$, $pK_1 = 6.9$, and $pK_2 = 9.7$.

Table 1: Data Collection and Atomic Model Statistics

parameters	T50V	Y42F
data collection		
resolution (Å)	1.15	1.10
observations	116065	186098
unique reflections	35299	40647
I/σ	34.9	24.0
completeness (%)	96.2	99.5
final shell	83.6	99.0
R_{sym} (%)	3.9	9.8
final shell	7.2	39.0
mosaicity	0.18	0.45
refinement		
reflections (all)	33533	38062
R-value	0.132	0.127
R_{free}	0.176	0.171
protein atoms	994	999
solvent atoms	109	104
rms deviation		
bond lengths (Å)	0.014	0.014
angular distances (Å)	0.033	0.035

removed (see Figure 5a). Diffraction data collection and atomic model statistics are given in Table 1. The active site of the Y42F mutant is shown in Figure 10a and compared with wild-type PYP. Due to the removal of the hydrogen bond to the chromophore in the Y42F mutant, the aromatic headgroup of the chromophore moves by 0.78 Å and forms a new but weaker hydrogen bond to the OH group of T50 (2.79 Å). In the mutant T50V (Figure 10b), the replacement of the hydroxyl group by a methyl group destroys the hydrogen bonds with the backbone carbonyl oxygen of E46 and the hydroxyl group of Y42, which leads to a very small decrease in the length of the hydrogen bond between its phenolate oxygen and the hydroxyl group of Y42 from 2.71 to 2.62 Å.

DISCUSSION

Spectral Tuning of the Ground-State Absorption Spectrum. For visual pigments and chromoproteins such as PYP that are involved in biological light sensing, it is important that the protein responds to light in the appropriate part of the spectrum. The absorption maximum of the anionic *p*-hydroxycinnamoyl chromophore in PYP's binding pocket at 446 nm is strongly red shifted from that of the free protonated chromophore at about 300 nm (*6*). The latter is shifted to 340 nm upon formation of the thiol ester bond with C69 and is further shifted to 398 nm upon deprotonation of the phenolic oxygen (*6*). The shift from 398 to 446 nm, accounting for 2700 cm^{-1} or about 25% of the whole red shift, is attributed to specific interactions with the protein environment. A comparable red shift of the absorbance maximum of a protonated Schiff base at 440 nm in methanol to the wavelength of maximal visible absorbance in the native protein is known as the opsin shift for retinal pigments (*35*). The high-resolution X-ray structure of the PYP ground state suggested an essential role for active site residues E46, R52, Y42, and T50 in spectral tuning of the chromophore's absorbance and stabilization of its negative charge (*12*). The phenolate oxygen of the chromophore hydrogen bonds to Y42 (2.71 Å) and E46 (2.69 Å). The side chain of T50 forms a hydrogen bond with the hydroxyl group of Y42 (2.83 Å) and the carbonyl oxygen of E46 (3.07 Å); its main-chain carbonyl oxygen also hydrogen bonds with R52 (2.97 Å), which shields the chromophore from solvent. The roles of residues E46 and R52 have been examined using site-directed mutants (*17*, *18*, *20*, *36*). It was shown that electrostatic interactions of the negatively charged chromophore with the positively charged guanidinium group of R52 make only a negligible contribution to the red shift of the chromophore absorption. The E46Q mutation, however, shifted the absorption peak by 777 cm^{-1} to 462 nm. Similar red shifts of 540 and 587 cm^{-1} are observed for the T50V and Y42F mutants, respectively, and indicate the importance of the hydrogen bond network around the chromophore for spectral fine-tuning of its absorption maximum. The red shifts of the absorption maxima can be explained on the basis of the crystal structures. The mutation Y42F destroys the hydrogen bonds between residue 42 and the chromophore as well as between residue 42 and T50. This leads to an increased distance between T50 and F42 due to van der Waals repulsion and movement of the chromophore's aromatic ring toward T50. A new but weaker hydrogen bond between the chromophore's phenolate oxygen and the hydroxyl group of T50 is formed (Figure 10a). The weakening of one hydrogen bond and the removal of the other lead to increased charge density on the chromophore which is known to red shift its absorption maximum (*6*). The mutation T50V destroys the hydrogen bonds with the backbone carbonyl oxygen of E46 and the hydroxyl group of Y42, resulting in van der Waals repulsion between Y42 and V50 but only very small changes in the chromophore coordinates (Figure 10b). Thus, T50 does not have a strong influence on the chromophore conformation but helps to dissipate negative charge via the hydrogen bond to Y42.

Origin of the 391 nm Spectral Shoulder in the Y42F Mutant. The absorption spectrum of the Y42F mutant is significantly different from that of wild type by a large 391 nm shoulder on the 458 nm maximum (Figure 2). A spectral shoulder (at ~350 nm) for the mutant M100A (*19*) increased on illumination, even with weak room light, and was ascribed to the steady-state accumulation of the I_2 photocycle intermediate. In contrast, the spectrum of Y42F was unaltered by exposure to room light or to overnight incubation in the dark. However, the spectrum of Y42F was sensitive to solvent and temperature. The disappearance of the 391 nm

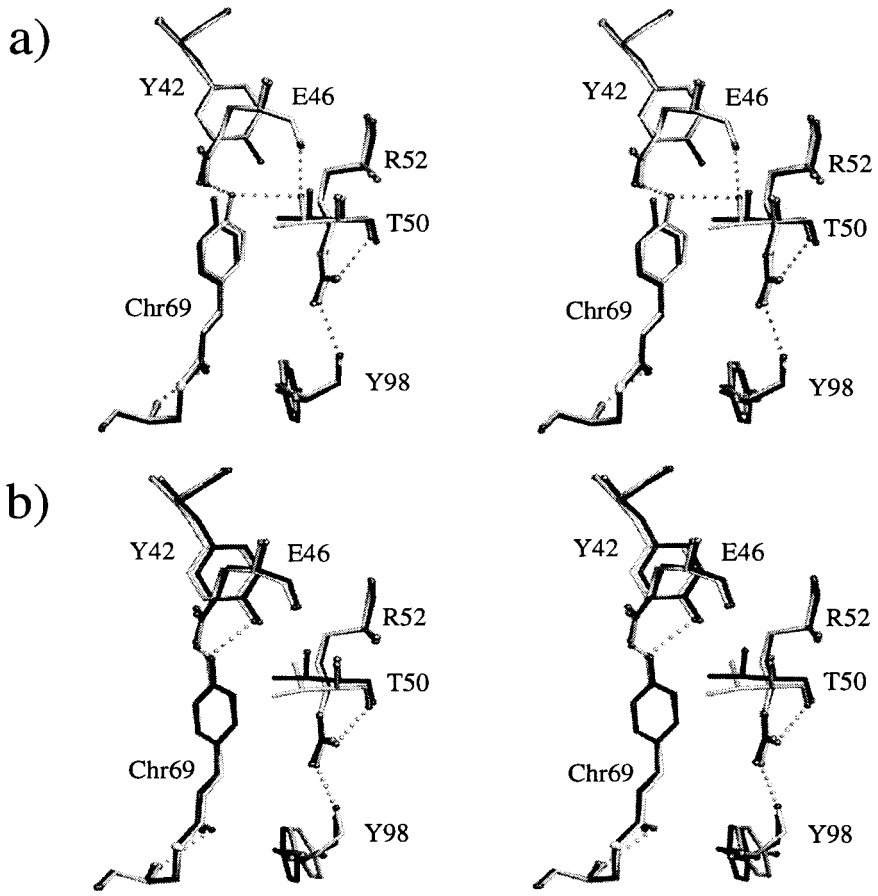

FIGURE 10: Stereoviews of the active sites of (a) wild-type PYP (dark) and the mutant Y42F (light) and (b) wild-type PYP (dark) and the mutant T50V (light). Wild-type PYP and the mutants are superimposed on the Cα carbons. The light dots represent the hydrogen bond network in the mutants Y42F and T50V, respectively. PDB codes are 2PHY, 1F98, and 1F9I for the coordinates of wild-type PYP, PYP T50V, and PYP Y42F, respectively.

band at −196 °C (unpublished observation) excludes the possibility that it is due to the vibrational fine structure of this mutant since this should not be sensitive to temperature. Upon denaturation with guanidine hydrochloride, the 391 nm band formed as a stable intermediate at about 1.1 M guanidine before the protein unfolded at 2.2 M guanidine as indicated by the generation of the 340 nm band (Figure 3). The 391 nm shoulder thus represents a second chromophore conformation within the protein population. The absorption maximum at 391 nm indicates that it is clearly distinct from denatured PYP.

The effects of chaotropic and kosmotropic agents were different from those of denaturants. Kosmotropes such as $(NH_4)_2SO_4$ are well-known stabilizers of proteins and are routinely used for their storage. They increase the ionic strength of a solution and enhance water clusters around proteins, thereby decreasing the entropy of water and the total free energy of the system (*32*). Thus, kosmotropes make proteins more compact by salting out hydrophobic residues. Application of $(NH_4)_2SO_4$ to PYP Y42F reduced the size of the 391 nm shoulder by stabilization of the main species absorbing at 458 nm (Figure 5a). In contrast, the chaotrope NH_4Cl destabilized the 458 nm species by increasing the amount of the 391 nm species (Figure 5b). Chaotropic agents bind extensively to the charged groups and dipoles (peptide bonds) of proteins, resulting in the destabilization of the protein by reduction of the number of water clusters around it (salting in) (*32*). It is interesting to note that neither NH_4Cl nor the strongest chaotrope thiocyanate (results not shown) denatures PYP Y42F completely, which would be indicated by a peak at 340 nm.

FT Raman spectroscopy, which selectively monitors the chromophore vibrations in the protein, provides direct evidence for two different chromophore conformations in the Y42F mutant. The main vibrational band at 1555 cm^{-1} with a shoulder at 1530 cm^{-1} in wild-type PYP (1552 and 1530 cm^{-1} in Y42F), analogous to the Y8a and Y8b modes of tyrosinate (*37*), shows a strong sideband at 1572 cm^{-1} in Y42F which is missing in the wild type as well as in the T50V mutant (Figure 6). The observation that the two bands at 1552 and 1572 cm^{-1} in Y42F change intensity in response to application of sulfate and chloride ions, respectively, qualitatively in the same way as the absorbance bands at 458 and 391 nm in the UV/vis spectrum, indicates that the 1552 and 1572 cm^{-1} bands represent two different chromophore conformations. The bands at 1555 and 1163 cm^{-1} in wild-type PYP (Figure 6a) are indicative for the protonation state of the chromophore (*34*). The resonance Raman spectrum of the chromophore model compound *p*-hydroxycinnamyl phenyl thioester in its anionic form shows corresponding bands at 1568 and 1166 cm^{-1}. In the neutral model compound, the band at 1568 cm^{-1} is shifted by 32 cm^{-1} to 1600 cm^{-1} and the band at 1166 cm^{-1} is shifted to 1176 cm^{-1} (*34*). The lack of a band at about 1176 cm^{-1} (Figure 6c) and the comparatively small shift of 20 cm^{-1} of the main peak (from 1552 to 1572 cm^{-1}) in the mutant Y42F (Figure

6c) suggest that the chromophore in the second conformation is not protonated. This is in agreement with a larger peak shift of 31 cm^{-1} (from 1552 to 1583 cm^{-1}) in the temperature-denatured Y42F mutant where the chromophore is protonated (unpublished observations) and with the acid titration of Y42F (Figure 4), which shows a biphasic transition with two pK_a values of 4.4 and 6.4.

Time-Resolved UV/Vis Spectroscopy. The kinetics of the bleach and recovery reactions in the PYP mutants T50V and Y42F at neutral pH are significantly different from those of the wild type but have changed by less than 1 order of magnitude. This relatively small effect was especially unexpected for Y42F, since Y42 is directly H-bonded to the chromophore hydroxylate (Figure 1). These results are similar to those for the R52A mutant (*17*) and to wild-type PYP in the presence of primary alcohols and urea (*8*, *38*). In all cases, the bleach becomes faster and the recovery slower, which correlates with a somewhat reduced stability of the protein. Accordingly, the midpoint for guanidine denaturation was decreased, and the pK_a for acid denaturation increased in the T50V and Y42F mutants when compared to the wild type. The observation that the effect of pH on the kinetics in T50V and Y42F is similar to that of wild-type PYP (Figures 8 and 9) suggests that T50 and Y42 are not directly involved in any protonation or deprotonation events that control the speed of the light cycle.

Fluorescence Spectroscopy. Evidence for the interconvertability of the two chromophore species in Y42F comes from the fluorescence data. Although the fluorescence emission spectrum of Y42F is very similar to that of the wild type and does not change when the excitation wavelength is varied from 320 to 450 nm, the fluorescence excitation spectrum differs from wild-type PYP by a shoulder at about 390 nm. This could be explained by two different protein populations in the Y42F sample with maximal absorbance at 391 and 458 nm and energy transfer from 391 to 458 nm if the protein was dimeric. The linear instead of an abrupt decrease in fluorescence emission in response to sample dilution, however, excludes this possibility. Hence, the 391 nm species appears to be converted to the 458 nm species during the excited-state lifetime, suggesting minimal structural rearrangements.

CONCLUSIONS

Our results demonstrate the importance of the hydrogen bond network around the chromophore for stabilization of the chromophore's negative charge and tuning of its absorption maximum in the ground state. In contrast to residues Y42 and E46, T50 is not directly hydrogen-bonded to the chromophore but together with these residues is involved in fine-tuning of its absorption maximum and helps to dissipate the negative charge located inside the protein. The small effects on the photocycle kinetics and the stability of the protein resulting from the T50V mutation are consistent with the observation that T50 is the only active site residue that is not conserved in the five known PYP sequences (*3*, *4*, *39*). Y42 is crucial for stabilizing the native conformation of the chromophore through hydrogen bonding. In the Y42F mutant, hydrogen bonds of the phenolic oxygen of Y42 with the T50 hydroxyl group and the phenolic oxygen of the chromophore are lost. This leads to a second chromophore conformation in the ground state and a destabilized and possibly less rigid protein. The interconversion between the two chromophore forms is fast relative to fluorescence emission, implying only small structural changes. The blue shift of the chromophore absorption to 391 nm could be explained by (i) a movement of the chromophore toward the positively charged R52, (ii) chromophore protonation or stronger hydrogen bonding to the phenolic oxygen of the chromophore, and/or (iii) redistribution of the electron density among the atoms of the chromophore due to changes in the chromophore's environment or in its geometry or conjugation. The double mutant Y42F/R52A, which shows an absorption maximum at 458 nm and an even further blue-shifted shoulder at 375 nm (unpublished observations), excludes explanation i. The Raman spectra, the photoexcitability, and the acid titration curves suggest that the second chromophore conformation is not fully protonated. A possible interpretation is that the hydrogen bonds to the phenolate oxygen of the chromophore differ in the two forms. Either shorter hydrogen bonds or geometrical changes leading to greater orbital overlap would reduce the electron density on the phenolic oxygen and blue shift the absorption maximum. It is also possible that the reduced stability of the protein allows the penetration of one or more water molecules into the active site. This could lead to the formation of an additional hydrogen bond between the chromophore and a water molecule or to a change in the acidity of the E46 carboxyl group via an increase in hydration or dielectric constant in the immediate vicinity of the E46−chromophore hydrogen bond.

ACKNOWLEDGMENT

We thank Christopher Putnam for collection of the diffraction data of PYP T50V and Dr. Benedikt Hessling for help with FT Raman spectroscopy. Diffraction data for T50V were collected at the Cornell High Energy Synchrotron Source (CHESS), and diffraction data for Y42F were collected at the Stanford Synchrotron Radiation Laboratory (SSRL), which is operated by the Department of Energy, Office of Basic Energy Sciences.

REFERENCES

1. Meyer, T. E. (1985) *Biochim. Biophys. Acta 806*, 175−183.
2. Meyer, T. E., Fitch, J. C., Bartsch, R. G., Tollin, G., and Cusanovich, M. A. (1990) *Biochim. Biophys. Acta 1016*, 364−370.
3. Kort, R., Phillips-Jones, M. K., van Aalten, D. M. F., Haker, A., Hoffer, S. M., Hellingwerf, K., and Crielaard, W. (1998) *Biochim. Biophys. Acta 1385*, 1−6.
4. Jiang, Z. Y., Swem, L. R., Rushing, B. G., Devanathan, S., Tollin, G., and Bauer, C. E. (1999) *Science 285*, 406−409.
5. Sprenger, W. W., Hoff, W. D., Armitage, J. P., and Hellingwerf, K. J. (1993) *J. Bacteriol. 175*, 3096−3104.
6. Baca, M., Borgstahl, G. E. O., Boissinot, M., Burke, P. M., Williams, D. R., Slater, K. A., and Getzoff, E. D. (1994) *Biochemistry 33*, 14369−14377.
7. Hoff, W. D., Düx, P., Hård, K., Devreese, B., Nugteren-roodzant, I. M., Crielaard, W., Boelens, R., Kaptein, R., van Beeumen, J., and Hellingwerf, K. J. (1994) *Biochemistry 33*, 13959−13962.
8. Meyer, T. E., Yakali, E., Cusanovich, M. A., and Tollin, G. (1987) *Biochemistry 26*, 418−423.
9. Hoff, W. D., van Stokkum, I. H., van Ramesdonk, H. J., van Brederode, M. E., Brouwer, A. M., Fitch, J. C., Meyer, T. E., van Grondelle, R., and Hellingwerf, K. J. (1994) *Biophys. J. 67*, 1691−1705.

10. Ujj, L., Devanathan, S., Meyer, T. E., Cusanovich, M. A., Tollin, G., and Atkinson, G. H. (1998) *Biophys. J. 75*, 406−412.
11. Devanathan, S., Pacheco, A., Ujj, L., Cusanovich, M., Tollin, G., Lin, S., and Woodbury, N. (1999) *Biophys. J. 77*, 1017−1023.
12. Borgstahl, G. E. O., Williams, D. R., and Getzoff, E. D. G. (1995) *Biochemistry 34*, 6278−6287.
13. Düx, P., Rubinstenn, G., Vuister, G. W., Boelens, R., Mulder, F. A. A., Hård, K., Hoff, W. D., Kroon, A. R., Crielaard, W., Hellingwerf, K. J., and Kaptein, R. (1998) *Biochemistry 37*, 12689−12699.
14. Genick, U. K., Borgstahl, G. E. O., Ng, K., Ren, Z., Pradervand, C., Burke, P. M., Srajer, V., Teng, T.-Y., Schildkamp, W., McRee, D. E., Moffat, K., and Getzoff, E. D. (1997) *Science 275*, 1471−1475.
15. Genick, U. K., Soltis, S. M., Kuhn, P., Canestrelli, I. L., and Getzoff, E. D. (1998) *Nature 392*, 206−209.
16. Perman, B., Srajer, V., Ren, Z., Teng, T., Pradervand, C., Ursby, T., Bourgeois, D., Schotte, F., Wulff, M., Kort, R., Hellingwerf, K., and Moffat, K. (1998) *Science 279*, 1946−1950.
17. Genick, U. K., Devanathan, S., Meyer, T. E., Canestrelli, I. L., Williams, E., Cusanovich, M. A., Tollin, G., and Getzoff, E. D. (1997) *Biochemistry 36*, 8−14.
18. Mihara, K., Hisatomi, O., Imamoto, Y., Kataoka, M., and Tokunaga, F. (1997) *J. Biochem. 121*, 876−880.
19. Devanathan, S., Genick, U. K., Canestrelli, I. L., Meyer, T. E., Cusanovich, M. A., Getzoff, E. D., and Tollin, G. (1998) *Biochemistry 37*, 11563−11568.
20. Devanathan, S., Brudler, R., Hessling, B., Woo, T. T., Gerwert, K., Getzoff, E. D., Cusanovich, M. A., and Tollin, G. (1999) *Biochemistry 38*, 13766−13772.
21. Kroon, A. R., Hoff, W. D., Fennema, H. P., Gijzen, J., Koomen, G. J., Verhoeven, J. W., Crielaard, W., and Hellingwerf, K. J. (1996) *J. Biol. Chem. 271*, 31949−31956.
22. Devanathan, S., Genick, U. K., Getzoff, E. D., Meyer, T. E., Cusanovich, M. A., and Tollin, G. (1997) *Arch. Biochem. Biophys. 340*, 83−89.
23. Studier, F. W., Rosenberg, A. H., Dunn, J. J., and Dubendorff, J. W. (1990) *Methods Enzymol. 185*, 60−89.
24. Simondsen, R., and Tollin, G. (1983) *Biochemistry 22*, 3008−3016.
25. Meyer, T. E., Tollin, G., Causgrove, T. P., Cheng, P., and Blankenship, R. E. (1991) *Biophys. J. 59*, 988−991.
26. Demas, J. N., and Crosby, G. A. (1971) *J. Phys. Chem. 75*, 991−1024.
27. Pace, C. N. (1975) *CRC Crit. Rev. Biochem. 3*, 1−43.
28. Otwinowski, Z., and Minor, W. (1997) *Methods Enzymol. 276*, 307−326.
29. Navaza, J. (1994) *Acta Crystallogr. A50*, 157−163.
30. Sheldrick, G. M., and Schneider, T. R. (1997) *Methods Enzymol. 277*, 319−343.
31. Hofmeister, F. (1888) *Naunyn-Schmiedeberg's Arch. Pathol. 24*, 247−260.
32. Baldwin, R. L. (1996) *Biophys. J. 71*, 2056−2063.
33. Gerwert, K. (1995) in *Infrared and Raman Spectroscopy* (Schrader, B., Ed.) pp 617−640, VCH−Verlagsgesellschaft, Weinheim.
34. Kim, M., Mathies, R. A., Hoff, W. D., and Hellingwerf, K. J. (1995) *Biochemistry 34*, 12669−12672.
35. Nakanishi, K., Baloch-Nair, V., Arnaboldi, M., Tsujimoto, T., and Honig, B. (1980) *J. Am. Chem. Soc. 102*, 7945−7947.
36. Mataga, N., Chosrowjan, H., Shibata, Y., Imamoto, Y., and Tokunaga, F. (2000) *J. Phys. Chem. B 104*, 5191−5199.
37. Harada, I., and Takeuchi, H. (1986) in *Spectroscopy of Biological Systems* (Clark, R. J. H., and Hester, R. E., Eds.) Vol. 13, Chapter 3, John Wiley & Sons, Chichester.
38. Meyer, T. E., Tollin, G., Hazzard, J. H., and Cusanovich, M. A. (1989) *Biophys. J. 56*, 559−564.
39. Koh, M., van Driessche, G., Samyn, B., Hoff, W. D., Meyer, T. E., Cusanovich, M. A., and van Beeumen, J. J. (1996) *Biochemistry 35*, 2526−2534.

BI0009946